UNIVERSITY *of York*

This is a repository copy of *Sensitivity of detachment extent to magnetic configuration and external parameters*.

White Rose Research Online URL for this paper:
https://eprints.whiterose.ac.uk/id/eprint/99284/

Version: Accepted Version

Article:

White Rose
university consortium
Universities of Leeds, Sheffield & York

eprints@whiterose.ac.uk
https://eprints.whiterose.ac.uk/

Sensitivity of detachment extent to magnetic configuration and external parameters

Bruce Lipschultz[1], Felix I. Parra[2,3] and Ian H. Hutchinson[4]

E-mail: `bruce.lipschultz@york.ac.uk`
[1]York Plasma Institute, University of York, Heslington, York, YO10 5DQ, UK
[2]Rudolf Peierls Centre for Theoretical Physics, University of Oxford, Oxford, OX1 3NP, UK
[3]Culham Centre for Fusion Energy, Abingdon, OX14 3DB, UK
[4]Plasma Science and Fusion Center, Massachusetts Institute of Technology, Cambridge, MA 02139, USA

Abstract. Divertor detachment may be essential to reduce heat loads to magnetic fusion tokamak reactor divertor surfaces. Yet in experiments it is difficult to control the extent of the detached, low pressure, plasma region. At maximum extent the front edge of the detached region reaches the x-point and can lead to degradation of core plasma properties. We define the 'detachment window' in a given position control variable C (for example, the upstream plasma density) as the range in C within which the front location can be stably held at any position from the target to the x-point; increased detachment window corresponds to better control. We extend a 1D analytic model[1] to determine the detachment window for the following control variables: the upstream plasma density, the impurity concentration and the power entering the scrape-off layer (SOL). We find that variations in magnetic configuration can have strong effects; Increasing the ratio of the total magnetic field at the x-point to that at the target, $B_\times/B_t$, (total flux expansion, as in the Super-X divertor configuration) strongly increases the detachment window for all control variables studied, thus strongly improving detachment front control and the capability of the divertor plasma to passively accommodate transients while still staying detached. Increasing flux tube length and thus volume in the divertor, through poloidal flux expansion (as in the snowflake or x-divertor configurations) or length of the divertor, also increases the detachment window, but less than the total flux expansion does. The sensitivity of the detachment front location, z_h, to each control variable, C, defined as $\partial z_h/\partial C$, depends on the magnetic configuration. The size of the radiating volume and the total divertor radiation increase $\propto (B_\times/B_t)^2$ and $\propto B_\times/B_t$, respectively, but not by increasing divertor poloidal flux expansion or field line length. We believe this model is applicable more generally to any thermal fronts in flux tubes with varying magnetic field, and similar sources and sinks, such as detachment fronts in stellarator divertors and solar prominences in coronal loops.

1. Introduction

Divertor detachment is of central importance for practical tokamak reactor designs. It refers to strong dissipation of the parallel heat exhaust, including pressure loss, before it reaches the divertor surface. Detachment has been shown to give large reductions of up to a factor of 100 in electron pressure at the target, p [2, 3, 4], and similar drops in parallel heat flux at the target, $q_{||} \propto pT^{1/2}$, and ion flux to the target, $\Gamma_i \propto pT^{-1/2}$. However, as we move towards building a reactor, larger and larger parallel heat fluxes entering the divertor are anticipated and dissipating them becomes more difficult. It therefore becomes all the more urgent to understand whether and how divertor detachment can be controlled so that it dissipates high power densities without degrading the core confinement.

The detachment first starts at the divertor target, where the temperature is lowest. An approximately uniform low-pressure and temperature region then expands away from the target along the field. We call the upstream end of that cold region the 'detachment front' or interchangeably 'thermal front' as they are contiguous. The thermal front is a region of steep temperature gradients in which the electron temperature transitions between the hotter upstream region and the colder region below which is dominated by ionization, recombination and other neutral processes. The detachment front is often observed to move all the way to the x-point (fully-detached). (It can move further, forming poloidal detachment in the main chamber, but this is observed less frequently.) The presence of a low-temperature region at the x-point can lead to varying degrees of core energy confinement degradation [5, 6, 7, 8, 9, 10, 2, 11, 12, 4, 13]; either directly by introducing a cold region next to, or inside the separatrix; or indirectly, through easier penetration of neutrals and impurities across the separatrix [14, 5, 15, 16, 7, 2, 4, 13, 17]. The compression/enrichment of impurities and neutrals in the divertor has also been found to degrade during detachment [18, 19, 20, 21, 22], raising concerns for pumping He in a reactor when the divertor is fully-detached.

The ITER design balances the trade-off between core and divertor performance by keeping the detachment front close to the outer target, $\sim 15\%$ of the poloidal distance from target to x-point along the outer separatrix[23]. This conservatively keeps the cold detachment front far from the core plasma and leads to very good He compression and pumping. The predicted target heat flux reduction at the plate is of order a factor of 40[24], enough to keep heat fluxes below 10MW/m^2, but less than could be achieved – an appropriately conservative scenario. Feedback control of the detachment front location is a requirement to maintain any such divertor solution.

There have been several successful detachment feedback control experiments using impurity seeding gases for control of outer divertor detachment in H-mode plasmas [6, 7, 25, 26]. The main differences between those impurity seeding feedback techniques relates to the measurement, or metric, used to determine the appropriate flow of seeding gas. For example, using bolometer chords passing near the x-point allows the detachment front location to reach the region of the x-point [7], but no further. On the other hand, using target thermoelectric currents (correlated with T_e assuming that the inner divertor is already detached) leads to the detachment front being held near to the target (or on the verge of detachment)[6, 25, 26], more similar to the ITER scenario. To our knowledge

there has been little study of how feedback control can be used to hold the detachment front at any chosen position ranging from target to x-point. This prevents the study of the dependence of the front location in the divertor proper (as opposed to the region of the x-point[13]) on core and divertor performance, which would (a) be useful in studying the trade-off between core and divertor performance; and (b) is likely important for ITER and DEMO. Ultimately, we need to determine if there is a core (radiation, dilution and confinement) and divertor (power loss, detachment, etc.) scenario that is compatible with a cost-effective, energy-producing, controllable reactor, and that allows control of detachment.

The difficulty of holding the front location at a given point within the divertor proper appears to be due to the sensitivity of its location to control variables such as upstream separatrix density n_u, impurity seeding rate, or/and power flowing into the SOL, P_{SOL}. A review of the literature has not found studies specifically aimed at characterizing and understanding that sensitivity, as opposed to stability. However, we have found published data which can give us some guidance. Early Ohmic C-Mod studies of the detachment threshold, as measured by Langmuir probes, showed that the range of upstream density, n_u, between start of detachment at the target, n_{ut}, and detachment reaching the x-point, $n_{u\times}$, is small. We call the range $n_{u\times} - n_{ut}$ the 'detachment window' in n_u. It ranged from $n_{u\times} - n_{ut} \sim 0.05 n_{ut}$ (figure 21 in reference [2]) to $0.2 n_{ut}$ (figure 3 in reference [2]). A more recent DIII-D study[27], employing divertor Thomson scattering, also indicates a small detachment window in upstream density for H-mode plasmas at each of several different levels of injected neutral beam power. A more localized way of quantifying the sensitivity of detachment front location to control variables, C (e.g. n_u), is to define a front sensitivity to a particular control variable as $\partial z_h / \partial C$, where z_h is the front location.

The present work provides theoretical predictions of the detachment position dependence on plasma parameters, based on further development of an analytic model by Hutchinson for one-dimensional thermal fronts[1]. For conventional divertors with vertical divertor plate (e.g. C-Mod, ASDEX-Upgrade, JET and ITER) and flat plate (e.g. DIII-D and JET), the model predicts, consistent with the experimental data above, a fairly narrow window in detachment for upstream density. We compare the predicted detachment windows and $\partial z_h / \partial C$ for $C = n_u$, P_{SOL} and fractional impurity concentration, f_I (related to seeding rate). We present equations representing the extent to which the detachment front sensitivity and detachment window are modified by changing the divertor characteristics: particularly the variation of the total magnetic field, B, in the divertor, and the field line length from upstream to target, L, emblematic of 'unconventional' divertors such as 'snowflake'[28], 'x-divertor'[29] and 'super-x'[30] divertor configurations. We find that decreasing total magnetic field strength B from x-point $(B_\times)$ to target (B_t) strongly increases the detachment window for all control variables. The front location sensitivity to control variables also decreases. Increasing field line length in the divertor, either by poloidal flux expansion or increasing the divertor depth, also enhances the detachment window, but not as strongly.

The underlying physics in the above enhancements is as follows: the gradient in the total field, ∇B, pointing towards the x-point, also creates a $\nabla q_\parallel$ in the same direction due to changes in the flux tube area $(\propto 1/|B|)$. If the front moves towards the x-point

due to increased radiation such a $\nabla q_\parallel$ reduces the distance the front moves before finding a new equilibrium between increased radiation and $q_\parallel$, thus increasing the detachment window and detachment front control. The variation in total B (total flux expansion) has other important consequences beyond detachment control: The radiating volume increases proportional to $(B_\times/B_t)^2$ due to both the radiating region length and area scaling as $B_\times/B_t$. Overall this leads to an increase in the total radiation proportional to $B_\times/B_t$. On the other hand increasing the fraction of overall flux tube length in the divertor, $z_\times/L$, does not increase the radiating volume, but it affects the front location control by modifying the temperature profile upstream of the front. We discuss in detail these two different effects in subsection 6.2.

The detailed physics of divertors and detachment includes both complicated atomic physics and multi-dimensional transport effects. The effect of atomic physics on detachment has been considered in 2D models with full divertor geometry [31, 32], simplified 2D slab models [33] and 1D models [34, 35, 36, 37]. In all these models, charge exchange collisions and recombination are important to explain the pressure drop between the X-point and the divertor plates. Such processes have a significant but more limited influence on the energy losses, which include radiation of both impurities and hydrogen [31, 32]. It is generally assumed that the impurity radiation dominates, but in some cases, the radiation due to hydrogen, aided by very effective recombination, has been reported to be more important for energy loss [31]. Even when impurity radiation dominates and is localized in a thin thermal front, theoretical arguments and numerical evidence suggest that 2D geometrical effects can be important to reproduce observations [38, 39]. In 1D models, charge exchange collisions appear to be an energy dissipation mechanism comparable to radiation [34, 36], although these models tend to overpredict the effect of charge exchange losses by assuming that all charge exchanged ions carry their entire energy and momentum directly to surrounding surfaces.

In our model we intentionally avoid having to understand and calculate the more complicated neutral effects in the cold region below the thermal front. We do this by focussing our attention on the thermal front itself, where the electron temperature is dropping due to radiation that we take to be mostly from impurities (but could include hydrogen energy losses and neutral enhancement). The simple rationale for this model is that bringing the electron temperature down to the few eV level at the downstream end of the thermal front is a necessary condition for detachment. The complicated processes that occur beyond the thermal front (e.g. recombination), are important in terms of particle, momentum, and possibly energy loss, but are ignored here to allow us to derive a robust, informative model of detachment front location. We believe that their inclusion will not change the general physics we have uncovered, namely the importance of magnetic configuration on detachment control, and the relative sensitivity of the detachment front location to external variables. Rather their inclusion will lead to a more realistic profile of plasma characteristics between the thermal front and the target. The limitations of the method will be discussed further in subsection 6.3.

2. Review of the thermal front model

The one-dimensional treatment balances the divergence of parallel conduction with the net volumetric energy input $H = S - E$ where S is the source of energy (composed mostly of perpendicular heat fluxes), and E is the emissive energy loss by radiation. Paper [1] may be consulted for more details than we provide here. The equation expressing this balance is

$$\nabla \cdot \left(\frac{\boldsymbol{B}}{B} \kappa_\parallel \frac{\boldsymbol{B}}{B} \cdot \nabla T \right) = -H, \tag{1}$$

where $\kappa_\parallel$ is the Spitzer parallel conductivity. The divergenceless nature of $\boldsymbol{B}$, $\nabla \cdot \boldsymbol{B} = 0$, means that ∇ and $\boldsymbol{B}$ commute, that is, $\nabla \cdot (\boldsymbol{B} g) = \boldsymbol{B} \cdot \nabla g$ for any g. Therefore this equation can be rearranged as

$$-H = B \frac{\boldsymbol{B}}{B} \cdot \nabla \left(\frac{1}{B} \kappa_\parallel \frac{\boldsymbol{B}}{B} \cdot \nabla T \right) = B \nabla_\parallel \left(\frac{1}{B} \kappa_\parallel \nabla_\parallel T \right) = B \frac{d}{dl} \left(\frac{\kappa_\parallel}{B} \frac{dT}{dl} \right), \tag{2}$$

where l is the length along the field line.

Detachment requires the target temperature to be $\lesssim 5$ eV. In our model that translates to a strong radiative loss E, giving a region of negative H (see Figure 1 for a 1D illustration of a temperature profile along with source and sink). The impurity radiation that we suppose dominates this term is generally well represented for impurity I as the product $n_e n_I Q(T) = n_e^2 f_I Q(T)$: the square of the electron density times the impurity density fraction ($f_I = n_I/n_e$) times a "radiation function", Q, that depends on temperature. We assume the temperature dependence consists of a peak in the radiation at a particular temperature and falling to small levels at much higher or lower temperature. That is indeed the form of Q given by the standard collisional-radiative equilibrium[40], but we do not exclude other effects such as neutral charge-exchange or finite residency time.

The solutions to the heat conduction equation under those conditions give rise to a radiative region that is localized in position which we referred to earlier as the 'thermal front'. Figure 1 shows such a thermal front. On the cold side of the thermal front, there is a low temperature region with $T \sim T_c$ at which (in principle) $H = 0$. The hot edge of the front is taken to be at temperature T_h where the emissive loss becomes negligible. Above temperature T_h the heat conduction and heat source S determine the temperature's spatial dependence. To obtain the thermal front shown in Figure 1, we have assumed an upstream density $n_u = 10^{20}$ m^{-3}, upstream temperature $T_u = 110$ eV, connection length, L, of 26.5m and a nitrogen fraction $f_I = 0.04$. The cooling function for nitrogen that we have used is

$$Q = 5.9 \times 10^{-34} \frac{(T - 1 \, \text{eV})^{1/2} (80 \, \text{eV} - T)}{1 + 3.1 \times 10^{-3} (T - 1 \, \text{eV})^2} \, \text{W} \cdot \text{m}^3 \tag{3}$$

for 1 eV $< T < 80$ eV, and is $Q = 0$ for temperatures outside this range. Our simple cooling function is similar to that in Fig. 1 of reference [41] for nitrogen which includes non-coronal effects. Note that T_h of 65 eV in Fig. 1 has been chosen to be where the cooling curve Q drops to 5% of its maximum value. Larger values of T_h could be chosen, up to 80 eV.
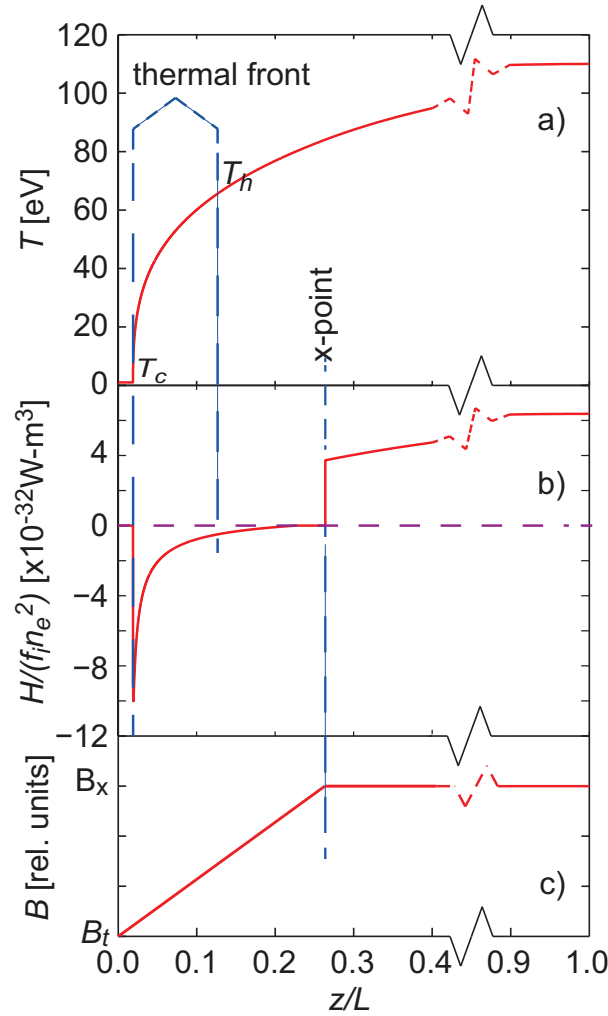
Figure 1. Profiles of a) thermal front solution to the conduction equation; b) the corresponding energy sources and sinks, H, normalized to $f_i n_e^2$ to enable the positive values of H at large z to be non-negligible in the figure; and c) the magnetic field magnitude assumed in the calculations. The coordinate along the magnetic field line z, closely related to the parallel length l, is defined in (4). The thermal front is demarcated by T_h and T_c, which correspond to z_h and z_c. Note that the cooling function utilized in this calculation is given in equation (3).

Following the derivation of [1], we define a convenient parallel coordinate z by

$$dz = \frac{B_\times}{B} dl = \frac{B_\times}{B_p} dl_p, \tag{4}$$

where l_p is the poloidal length, B_p is the poloidal magnetic field, and $B_\times$ is any reference value of the total field magnitude (we take it here to be the value at the x-point). We take $z = 0$ at the target, and use subscripts t for values at the target, c and h at the cold and hot ends of the thermal front, $\times$ at the x-point, and u at the upstream end ($z = L$). *The length z is the volume of the flux tube contained between the divertor plate and the position of interest normalized by a reference area ($\propto 1/B_\times$).* Defining a scaled conductivity,

$$\kappa \equiv \kappa_\| B_\times^2 / B^2, \tag{5}$$

the conduction equation is simplified as

$$\frac{dq}{dz} = H = S - E, \tag{6}$$

where

$$q = -\kappa \frac{dT}{dz} = -\kappa_{\parallel} \frac{B_{\times}^2}{B^2} \frac{dT}{dz} = -\kappa_1 T^{5/2} \frac{B_{\times}^2}{B^2} \frac{dT}{dz} \tag{7}$$

using Spitzer conductivity $\kappa_{\parallel} = \kappa_1 T^{5/2}$. The quantity q is a scaled form of the parallel heat flux density: $q = q_{\parallel} B_{\times}/B$. Since the area of a flux tube varies inversely proportional to B, we can identify q as the total parallel heat flux (not the heat flux *density*, $q_{\parallel}$) through a flux tube which has unit area where $B = B_{\times}$. In the absence of sources and sinks q is constant and $q_{\parallel}$ varies as B. ‡

Paper [1] identifies the heat flux lost in the thermal front through a first integral of the conduction equation. Multiplying equation (6) by $q = -\kappa(dT/dz)$, and integrating in z starting from the cold end of the front, we obtain

$$\left[q^2\right]_{z_c}^z = -\int_{T_c}^T 2\kappa(T')H(T')dT' = 2f_I p^2 \int_{T_c}^T \kappa(T')\frac{Q(T')}{T'^2}dT', \tag{8}$$

where we have assumed that the electron pressure $p = n_e T$ is constant through the front, and we have approximated $H \simeq -E$, assuming radiation overwhelms the local source S in the thermal front. We have also assumed that f_I does not depend on temperature or position, and that Q only depends on position through the temperature (no localized enhancement due to transport times or neutrals). This approximation is valid if the front is thin compared to the characteristic length of variation in f_I and Q. The assumption that the front is thin is important because it allows the front to slide between the plate and the x-point. A thick front, approaching the size of the divertor, would not allow movement of the front - our emphasis here. Using equation (8), where we choose as upper limit of the integral the temperature $T = T_h$ at which the radiation falls to a negligible level, we find the relation between the heat flux q_h entering the hot side of the front and the heat flux q_c leaving the cold side, $q_h^2 - q_c^2 = 2f_I p^2 \int_{T_c}^{T_h} \kappa(T')Q(T')/T'^2 dT'$. We note that this formulation is the same as the one utilized for estimates of the maximum power that can be radiated along a field line [42, 43, 44, 41].

Formally within this analysis, the conductive heat flux leaving the front, q_c, is negligible because electron conduction is small at low temperature. Then, the heat flux dissipated in the front is

$$q_f = q_h \equiv -\left(\kappa\frac{dT}{dz}\right)_h \simeq -\sqrt{2f_I p^2 \int_{T_c}^{T_h} \kappa(T')\frac{Q(T')}{T'^2}dT'}. \tag{9}$$

For equilibrium, q_f must equal the heat flux entering the thermal front, q_i, which is due to sources upstream, that is:

$$q_i = -\left(\kappa\frac{dT}{dz}\right)_h = -\int_{z_h}^L Hdz \simeq -\int_{z_h}^L Sdz, \tag{10}$$

‡ In an axisymmetric (tokamak) configuration, we might consider two adjacent flux surfaces, separated by a small perpendicular distance $A_p/2\pi R$ to define the flux tube (so A_p is the total area between the flux surfaces). The volume $V = \int_0^{l_p(z)} A_p dl_p$ contained between them and bounded by the divertor plate ($z = 0$) and the position z, is $V = zB_p A_p/B_{\times}$, where $B_p A_p$ is (of course) invariant on flux surfaces. The total heat flux through A_p is $q_{\parallel} A_p B_p/B = q A_p B_p/B_{\times}$.

neglecting radiation losses above T_h. Note that both q_f and q_i are negative in this formulation. We denote the detachment front location by the hot end of the front, z_h, for ease of the analysis. z_c, and thus the detachment front, is a small distance away under the assumption that the front is thin.

The stability of the equilibrium $q_i = q_f$ depends on how the quantity $|q_i| - |q_f|$ changes with position. Consider a front located around the equilibrium position $z_h = z_{eq}$ for which

$$\frac{d}{dz_h}(|q_i| - |q_f|) \geq 0. \tag{11}$$

In this case, if the front is out of equilibrium at $z_h > z_{eq}$, the incoming power $|q_i|$ is larger than the power dissipated in the front, $|q_f|$, and the temperature in the SOL increases. Since the front is localized between T_c and T_h, and we have assumed in this section that $dT/dz \geq 0$, the front has to move towards the colder region, that is, back to $z_h = z_{eq}$. Thus, an equilibrium that satisfies (11) is stable to perturbations that drive the front to a position $z_h > z_{eq}$. A similar argument shows that a front that satisfies equation (11) is also stable to perturbation that move the front to a position $z_h < z_{eq}$. Conversely, a front that is around an equilibrium position $z_h = z_{eq}$ that satisfies

$$\frac{d}{dz_h}(|q_i| - |q_f|) < 0 \tag{12}$$

is unstable. If the front is at $z_h > z_{eq}$, the incoming power $|q_i|$ is smaller than the power dissipated in the front, $|q_f|$, the temperature in the SOL decreases, and the front moves to a higher z_h, further away from z_{eq}. Thus, equation (11) is the stability condition. Since in our model, both q_i and q_f are negative, condition (11) becomes

$$\frac{d}{dz_h}(q_i - q_f) \leq 0. \tag{13}$$

Although paper [1] included the important field-magnitude dependence for MARFEs [45, 46], its analysis of the case of divertor detachment approximated B as uniform over the entire field line length (not assumed in the current study). Paper [1] predicted that the range in upstream density where the detachment front is in the divertor (detachment window in n_u) is narrow and dependent on the fractional field line length in the main chamber $1 - z_\times/L$. The ratio of the upstream densities when the front is respectively at the x-point and the target was shown to be $n_{u\times}/n_{ut} = (1 - z_\times/L)^{-4/7}$. Numerically $n_{u\times}/n_{ut} = 1.23$ when $z_\times/L = 0.3$, which is in the range of C-Mod and DIII-D experimental observations mentioned earlier. The discussion in paper [1] presages our current work, saying 'The variation of κ proportional to $1/B^2$ produces a quite strong intrinsic variation, typically a factor of four in a conventional aspect-ratio tokamak SOL. This will tend to stabilize a front whose cold region is at larger major radius.' In the next section we make this stabilization effect explicit for divertor detachment and evaluate its strength.

3. Explicit inclusion of B-variation in the divertor

The unconventional divertor configurations referred to in the introduction have been advocated for their potential to enhance cross-field transport and radiating volume

at or below the x-point. In this study we emphasize instead evaluating how the various magnetic configuration characteristics modify the control of the location of the detachment front in the divertor by increasing divertor flux tube volume through (1) increasing divertor flux tube length (through poloidal flux expansion or longer divertor), and (2) total flux expansion due to B variation which increases the volume through increasing the area of the flux tube. In our 1D formulation, there is no distinction between increasing divertor flux tube volume and increasing $z_\times$.

The implicit presumption of the thermal front analysis is to suppose that the radiating (thermal front) region is sufficiently localized that certain parameters can be taken as uniform within it. We thus regard the field B, the pressure p, and the impurity fraction f_I as quantities that can be taken outside the integral of equation (9), to give

$$q_f = -\sqrt{2\kappa_1 f_I} \; n_u T_u \frac{B_\times}{B} \sqrt{\int_{T_c}^{T_h} T^{1/2} Q(T) \, dT}. \tag{14}$$

Here we have written the pressure in the front, $p = n_u T_u$, setting the pressure throughout the front equal to the upstream pressure, in the same spirit as the "two point model"[47, 48, 49, 50]. We are presuming any pressure loss due to atomic effects to occur in the cold region between the divertor plate and the cold end of the front. The final square root term is a constant that depends only on the radiating atomic species (modified perhaps by charge-exchange or non-equilibrium effects).

We now need to calculate self-consistently the incoming upstream heat flux q_i at the front, and also the upstream temperature T_u (and hence pressure, for a given n_u). In order to perform the required integrals we adopt model variations of S and B along z, given in expressions below. Other assumptions are possible but the simple expressions that we use are sufficient to represent the overall trends predicted by the thermal front model.

We approximate the cross-field divergence heat source, S, as uniform on field-lines adjacent to the core plasma, and zero in the divertor.

$$S = \begin{cases} 0 & \text{for } z < z_\times \\ S_0 & \text{for } z \geq z_\times \end{cases}. \tag{15}$$

This allows us to integrate the full conduction equation for the hot region above z_h (where E is negligible)

$$\frac{d}{dz}\left(\frac{\kappa_1 T^{5/2} B_\times^2}{B^2}\frac{dT}{dz}\right) = -S, \tag{16}$$

to find

$$\frac{2\kappa_1 B_\times^2}{7B^2}\frac{dT^{7/2}}{dz} = \begin{cases} S_0(L - z_\times) & \text{for } z < z_\times \\ S_0(L - z) & \text{for } z \geq z_\times \end{cases}. \tag{17}$$

We can immediately deduce that

$$q_i = -\begin{cases} S_0(L - z_\times) & \text{for } z_h < z_\times \\ S_0(L - z_h) & \text{for } z_h \geq z_\times \end{cases}. \tag{18}$$

The variation in q_i is shown in Figure 2, in which $-q_i$ increases through the SOL to the x-point and then stays constant through the divertor region.

In order to specify T_u we need a model for B. Since we are most interested in B variation in the divertor leg, we approximate the field variation as linear with z in the divertor leg but constant in the main chamber,

$$\frac{B}{B_\times} = \begin{cases} B_t/B_\times + (1 - B_t/B_\times)\, z/z_\times & \text{for } z < z_\times \\ 1 & \text{for } z \geq z_\times \end{cases} \tag{19}$$

(see figure 1(c)). We first integrate equation (17) between z and L. For $z \geq z_\times$, we find

$$\left[T^{7/2}\right]_z^L = \frac{7S_0}{2\kappa_1} \int_z^L (L - z')dz' = \frac{7S_0}{4\kappa_1}(L - z)^2, \tag{20}$$

recovering equation (16) of paper [1]. For $z < z_\times$, the integral becomes

$$\begin{aligned}
\left[T^{7/2}\right]_z^L &= \frac{7S_0}{2\kappa_1}\left[\int_z^{z_\times}\left(\frac{B(z')}{B_\times}\right)^2 (L - z_\times)dz' + \int_{z_\times}^L (L - z')dz'\right] \\
&= \frac{7S_0(L - z_\times)}{2\kappa_1}\left[\frac{z_\times}{3(1 - B_t/B_\times)}\left(1 - \left|\frac{B}{B_\times}\right|^3\right) + \frac{L - z_\times}{2}\right] \\
&= \frac{7S_0(L - z_\times)}{2\kappa_1}\left[\frac{z_\times - z}{3}\left(1 + \left|\frac{B}{B_\times}\right| + \left|\frac{B}{B_\times}\right|^2\right) + \frac{L - z_\times}{2}\right].
\end{aligned} \tag{21}$$

At positions far enough from the upstream end ($z = L$) that $(T/T_u)^{7/2}$ can be ignored, we can omit the lower limit in the left side of equations (20) and (21). So taking the lower limit to be $z = z_h$, giving the lowest temperature at which the equation applies, we obtain for the upstream temperature

$$T_u \simeq \left(\frac{7S_0}{4\kappa_1}\right)^{2/7}(L - z_h)^{4/7} \tag{22}$$

for $z_h \geq z_\times$, and

$$T_u \simeq \left(\frac{7S_0(L - z_\times)}{2\kappa_1}\right)^{2/7}\left[\frac{z_\times - z_h}{3}\left(1 + \left|\frac{B_h}{B_\times}\right| + \left|\frac{B_h}{B_\times}\right|^2\right) + \frac{L - z_\times}{2}\right]^{2/7} \tag{23}$$

for $z_h < z_\times$. In practice, we shall not analyze quantitatively cases where z is above the x-point, so we just use equation (23) for the remainder of the paper. The first term inside the brackets in equation (23), which originated from the integral $\int_{z_h}^{z_\times}\left(B/B_\times\right)^2 (L - z_\times)dz$, is fairly small compared to the second term, $(L - z_\times)/2$, when both $B_t^2/B_\times^2$ and $z_\times/L$ are small.

Substituting this T_u expression into equation (14) we get the front dissipation

$$q_f = -U\sqrt{f_I}\, n_u \frac{B_\times}{B_h}[S_0(L - z_\times)]^{2/7}\left[\frac{z_\times - z_h}{3}\left(1 + \left|\frac{B_h}{B_\times}\right| + \left|\frac{B_h}{B_\times}\right|^2\right) + \frac{L - z_\times}{2}\right]^{2/7}, \tag{24}$$

where the constant U is

$$U = 7^{2/7}(2\kappa_1)^{3/14}\sqrt{\int_{T_c}^{T_h} T^{1/2}Q(T)\, dT}. \tag{25}$$

An important characteristic of tokamak plasmas is the total power transported from the core plasma into the scrape off layer, often labeled P_{SOL}. For a characteristic exponential power scrape-off width λ_q, the parallel heat flux density near the separatrix

required to exhaust that power, when the poloidal field is B_p, is $q_\parallel = P_{\mathrm{SOL}}/(\lambda_q 2\pi R B_p/B)$. We may therefore identify $-q_i$ in our model with this expression, giving

$$S_0(L - z_\times) = \frac{P_{\mathrm{SOL}}}{\lambda_q 2\pi R B_p/B_\times}. \tag{26}$$

Thus $S_0(L - z_\times) \propto P_{\mathrm{SOL}}/\lambda_q$ when other geometrical parameters are constant. And this enables us to express the detachment sensitivity dependence on P_{SOL}.

Since equilibrium consists of the equality of $q_f(z_h)$ and $q_i(z_h)$ we can illustrate the solution by plotting both these quantities and observing that the front position is where they intersect. Figure 2 shows examples for a single value of S_0, determining $q_i(z_h)$, from equation (18). Two different cases for q_f from equation (24) are plotted, corresponding to different values of a control parameter, in this case n_u. The q_f curves are described by equation (24) below the x-point, $z_h < z_\times = 0.2L$. The part of the curves that corresponds to $z_h > z_\times$ is described by equation (14) with T_u given by (22). We do not consider the region $z_h > z_\times$ further because using the stability condition (13), one can see that the only stable solutions lie between the plate and the x-point. (As discussed in [1], other phenomena not accounted for here must be present to stabilize an x-point MARFE.) The extreme cases for which stable solutions exist are at the intersections of the q_f and q_i curves given in figure 2. These correspond to the intersection (detachment front) lying at the target plate ($z_h = 0$) or at the x-point $z_h = z_\times = 0.2L$. There is a continuum of stable solutions in between. The two subfigures compare a case with negligible field variation in the divertor $B_\times/B_t \to 1$ (figure 2a: which was the case considered in [1]) with a case where the target is at substantially smaller total field, $B_\times/B_t = 2$ (figure 2b), which is approximately equal to the major radius ratio $R_t/R_\times$ in a tokamak.

The solution at $z_h/L = 0.2$, $n_{u\times}$, corresponding to detachment front at the x-point, is the same in figures 2a and b (blue color in online document); the figures differ in the target solution. This is because of the large increase in $|q_f(0)| - |q_f(z_\times)|$ arising from B-variation in the divertor (see the effect of B_h in equation (24)). That leads to a much larger range in control parameters in figure 2b between the detachment front forming at the target and reaching the x-point. Thus n_u or f_I, (or P_{SOL} and hence S_0) or some combination thereof, can vary across a much larger detachment window in moving the front from the x-point to the plate. In other words the detachment window for each variable, or some combination of them, is much wider.

In figure 2b we have assumed that $B_\times/B_t > 1$. When the opposite is true (e.g. the inner divertor) and for sufficiently small $B_\times/B_t$, the variation in B becomes destabilizing. As we will see later, the exact value of $B_\times/B_t$ for there not to be a stable solution depends on $z_\times/L$.

4. Detachment window

In the previous section we have graphically found solutions for the upstream densities $n_{u\times}$ and n_{ut} for which the front is located at the x-point and the target, and thus we have obtained the detachment window in n_u. We have also qualitatively demonstrated the importance of $B_\times/B_t$ in increasing the detachment window in n_u. Here we derive formulae that show the explicit dependences of the detachment windows in several control
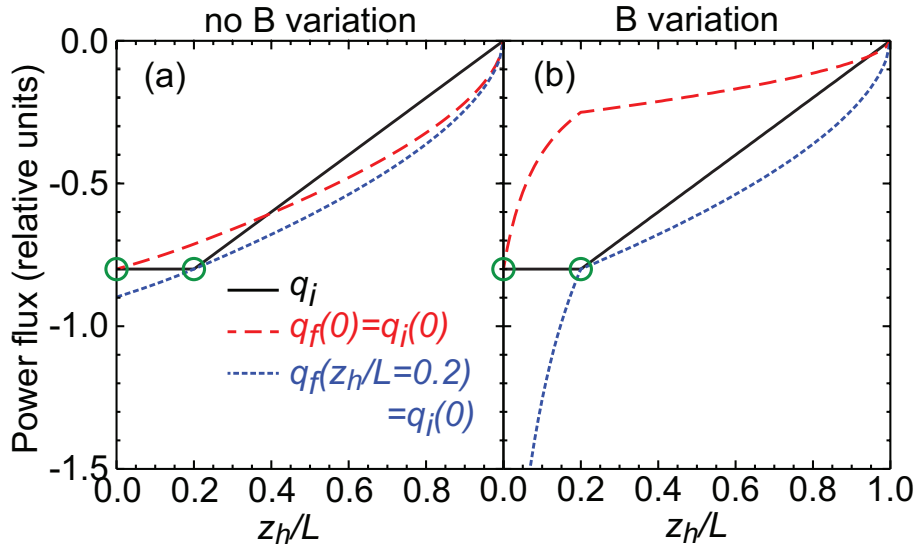
Figure 2. Sketch of the solutions to the equation $q_i(z_h) = q_f(z_h)$, represented by green circles, as a function of the front position z_h for: (a) Constant field, $B_\times/B_t = 1.0$ (equivalent to figure 5 of [1]), and (b) $B_\times/B_t = 2.0$. $q_i(z_h)$, given in equation (18) and represented here as a solid black line, is determined by the energy source S in (15). The function $q_f(z_h)$, represented by the dashed colored lines, is the heat flux dissipated by a front located at $z = z_h$. $q_f(z_h)$ is given by equation (24) below the x-point, $z_h < z_\times = 0.2L$, and by equation (14) with T_u given by (22) above the x-point, $z_h > z_\times$. Note that whereas there is only one curve $q_i(z_h)$ for fixed power into the SOL, P_{SOL}, the curves $q_f(z_h)$ depend on parameters such us the upstream density n_u, and thus there is a family of such curves. We choose to plot only two curves: in red, the cases with n_u such that the front is located at the divertor target, and in blue, the cases with n_u such that the front is located at the x-point.

variables on each other and on the effect of magnetic topology ($B_\times/B_t$, $L - z_\times$), starting first with n_u.

The first step is to set $q_i = q_f$ using equations (18) and (24). From that equality we can solve directly for n_u as a function of front position z_h/L (assumed $\leq z_\times$).

$$n_u = \frac{[S_0(L - z_\times)]^{5/7}}{U\sqrt{f_I}} \frac{B_h}{B_\times} \left[\frac{z_\times - z_h}{3} \left(1 + \left| \frac{B_h}{B_\times} \right| + \left| \frac{B_h}{B_\times} \right|^2 \right) + \frac{L - z_\times}{2} \right]^{-2/7}. \tag{27}$$

It is convenient to write this as a ratio of the density ($n_{u\times}$) when the front is at the x-point where $B = B_\times$, and (n_{uh}) when it is at some arbitrary position z_h where $B = B_h$:

$$\frac{n_{u\times}}{n_{uh}} = \frac{B_\times}{B_h} \left[\frac{2(z_\times - z_h)}{3(L - z_\times)} \left(1 + \left| \frac{B_h}{B_\times} \right| + \left| \frac{B_h}{B_\times} \right|^2 \right) + 1 \right]^{2/7}. \tag{28}$$

In particular, evaluating this density when the detachment front location, z_h, is at the target ($z_h = 0$, $n_{uh} = n_{ut}$ and $B_h = B_t$) we obtain the upstream density ratio corresponding to the two extremes of divertor front position (detachment window ratio)

$$\frac{n_{u\times}}{n_{ut}} = \frac{B_\times}{B_t} \left[\frac{2z_\times}{3(L - z_\times)} \left(1 + \left| \frac{B_t}{B_\times} \right| + \left| \frac{B_t}{B_\times} \right|^2 \right) + 1 \right]^{2/7}. \tag{29}$$
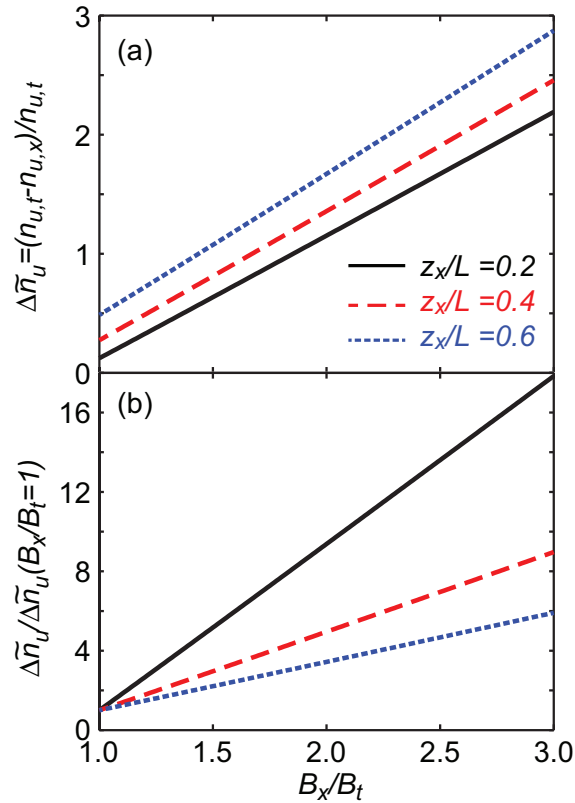
Figure 3. Effect of the variation in $B_\times/B_t$ and $z_\times/L$ on the size of the detachment window; a) detachment window, $\Delta\tilde{n}_u = n_{u\times}/n_{ut} - 1$, as a function of $B_\times/B_t$ for three cases of $z_\times/L$; b) the enhancement of the detachment window, for a given $B_\times/B_t$, over that for the case of $B_\times/B_t = 1$.

Including variation in B from the x-point to the target increases the ratio $n_{u\times}/n_{ut}$ approximately linearly with $B_\times/B_t$. As mentioned earlier, the density at which the front is at the x-point, $n_{u\times}$, is not affected by variation of B in the divertor, $B_\times/B_t$. Thus any change in the detachment window comes completely from decreases in n_{ut}.

The value of $B_\times/B_t$ can vary significantly from one magnetic configuration to another. In typical conventional divertors $B_\times/B_t$ is of order 1 to 1.3 which does not lead to a large effect. MAST-U[51], which is under construction, has $B_\times/B_t \sim 3$. TCV[52] allows for variations of up to $B_\times/B_t \sim 2$. The proposed Advanced Divertor Experiment (ADX)[53] has $B_\times/B_t \sim 2$. In general, lower aspect ratio tokamaks have the capability to achieve larger $B_\times/B_t$.

We denote the fractional detachment window as $\Delta\tilde{n}_u = (n_{u\times} - n_{ut})/n_{ut} = n_{u\times}/n_{ut} - 1$. Figure 3a illustrates $\Delta\tilde{n}_u$ from equation (29) for the range of $B_\times/B_t = 1-3$. We find that $\Delta\tilde{n}_u$ increases from 0.136 to 2.2 for $z_\times/L = 0.2$. The large enhancement of the detachment window over that for the $B_\times/B_t = 1$ case (a factor of ~ 18 for $B_\times/B_t = 3$) is shown in figure 3b. The effect of varying $z_\times/L$, shown in figure 3, is significant but smaller than changes brought about by a variation of $B_\times/B_t$. This points out that snowflake and x-divertor geometries, without significant variations in $B_\times/B_t$, should derive a modest enhancement of the detachment window over a conventional divertor by increasing $z_\times/L$. Of course, our simple model does not include the effect of
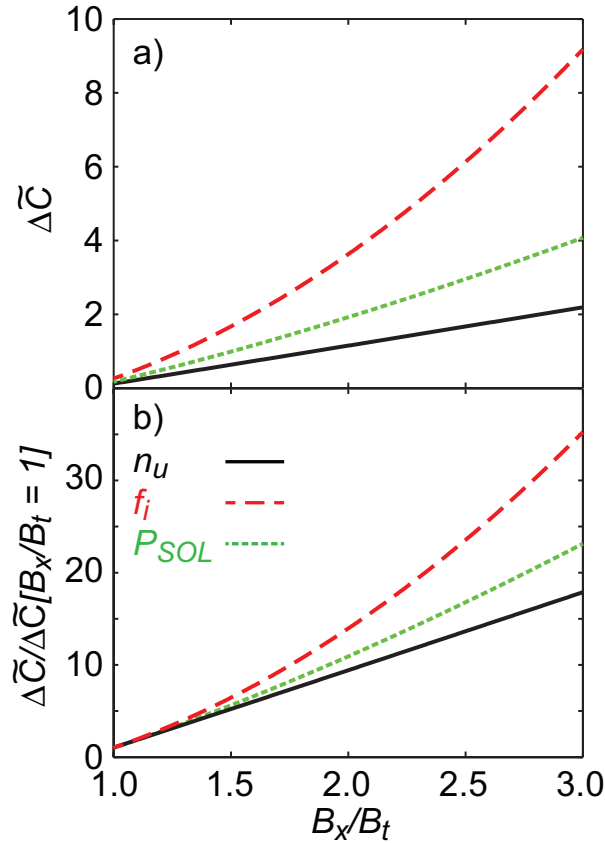
Figure 4. Extension of figure 3 to include all control variables for $z_\times/L = 0.2$: a) the increase in normalized detachment window, $\Delta\tilde{C}$, with changing $B_\times/B_t$ (the values of $\Delta\tilde{C}$ at $B_\times/B_t = 1$ are $\Delta\tilde{n}_u = 0.12$, $\Delta\tilde{f}_I = 0.26$ and $\Delta\tilde{P}_{\mathrm{SOL}} = 0.18$); b) all curves normalized to the case of $B_\times/B_t = 1$.

divertor target geometry and material which can affect neutral hydrogen and impurity sources and the resulting changes in the radiation contained in q_f. Our analysis also omits explicit localization, such as the interaction of neutrals with plasma in the region of poloidal flux expansion near the target (x-divertor) which Kotschenreuther et al have pointed out could reduce the 'tendency for the front to move upstream from the plate to the core X-point' [54].

The dependence of z_h on other control variables such as f_I or P_{SOL} (strictly $S_0(L - z_\times)$) can be treated in the same way as n_u. We denote the general control variable as $C = [n_u, f_I, P_{\mathrm{SOL}}(\text{or } S_0)]$. Setting $q_i = q_f$ and using equations (18) and (24), we find

$$\frac{C_\times}{C_h} = \left\{ \frac{B_\times}{B_h} \left[\frac{2(z_\times - z_h)}{3(L - z_\times)} \left(1 + \left| \frac{B_h}{B_\times} \right| + \left| \frac{B_h}{B_\times} \right|^2 \right) + 1 \right]^{2/7} \right\}^\beta, \qquad (30)$$

where the factor β is 1, 2 and -7/5 for $C = [n_u, f_I, P_{\mathrm{SOL}}(\text{or } S_0)]$, respectively. The detachment window ratio $C_\times/C_t$ is obtained by substituting $z_h = 0$, $B_h = B_t$. Note that while increases in f_I and n_u move the detachment front from the target to the x-point, decreases in P_{SOL} had the same effect; this is manifested in equation (30) with a negative β.

Figure 4 displays the scaling of the detachment window $\Delta\tilde{C} \equiv \max(C_\times, C_t)/\min(C_\times, C_t) -$
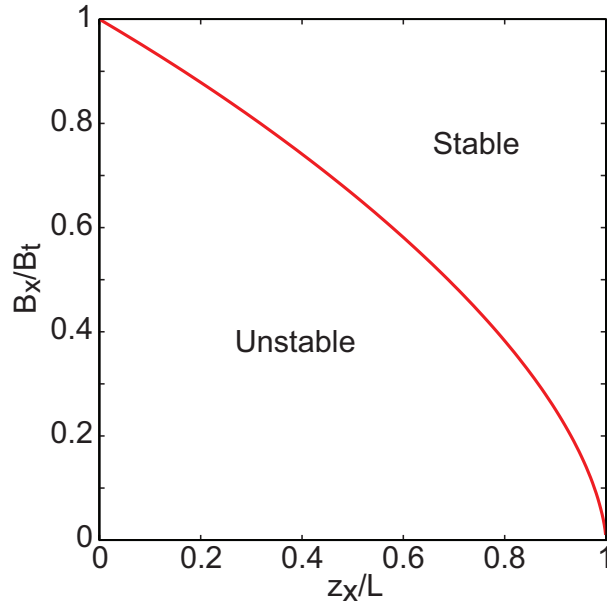
Figure 5. The minimum value of $B_\times/B_t$ for stable solutions of the detachment front location as a function of $z_\times/L$.

1, for n_u, f_I, and P_{SOL}. ($\Delta\tilde{n}_u = n_{u\times}/n_{ut} - 1$, $\Delta\tilde{f}_I = f_{I\times}/f_{It} - 1$, but $\Delta\tilde{P}_{\mathrm{SOL}} = P_{\mathrm{SOL}t}/P_{\mathrm{SOL}\times} - 1$). We have not included the effect of $z_\times/L$ as in figure 3. The detachment window in impurity seeding, $\Delta\tilde{f}_I$, has the strongest increase with increasing $B_\times/B_t$, scaling approximately quadratically with $B_\times/B_t$. The increase in the detachment window for P_{SOL} is of particular relevance for transients in core power loss (e.g. H-L energy confinement transitions or ELMs), which are ideally absorbed in the divertor plasma whilst keeping the divertor region detached and the detachment front in an optimal position.

At the end of section 3, we concluded that the detachment front location is unstable for sufficiently small $B_\times/B_t$. The transition to instability happens when the detachment window in any control variable disappears, that is, when $C_\times/C_t = 1$ in equation (30):

$$\frac{B_\times}{B_t}\left[\frac{2z_\times}{3(L - z_\times)}\left(1 + \left|\frac{B_t}{B_\times}\right| + \left|\frac{B_t}{B_\times}\right|^2\right) + 1\right]^{2/7} = 1. \tag{31}$$

This equation gives the minimum value that $B_\times/B_t$ must have for stability. We plot this minimum value as a function of $z_\times/L$ in figure 5. If for a given $z_\times/L$, we were to take a value of $B_\times/B_t$ below the curve in figure 5, the dependence of q_f on z_h would be such that the stability condition in equation (13) would not be satisfied. This stability limit for $B_\times/B_t$ is of importance for inner divertor regions where $B_\times/B_t$ can be of order 0.8 and $z_\times/L < 0.2$ leading to no stable solutions between the target and x-point; *the detachment front, once it starts at the target, should jump immediately to the x-point.*

5. Sensitivity to control variables

More than just the detachment window, the local sensitivity of the detachment front position to variations of the control variables C is important to the understanding of
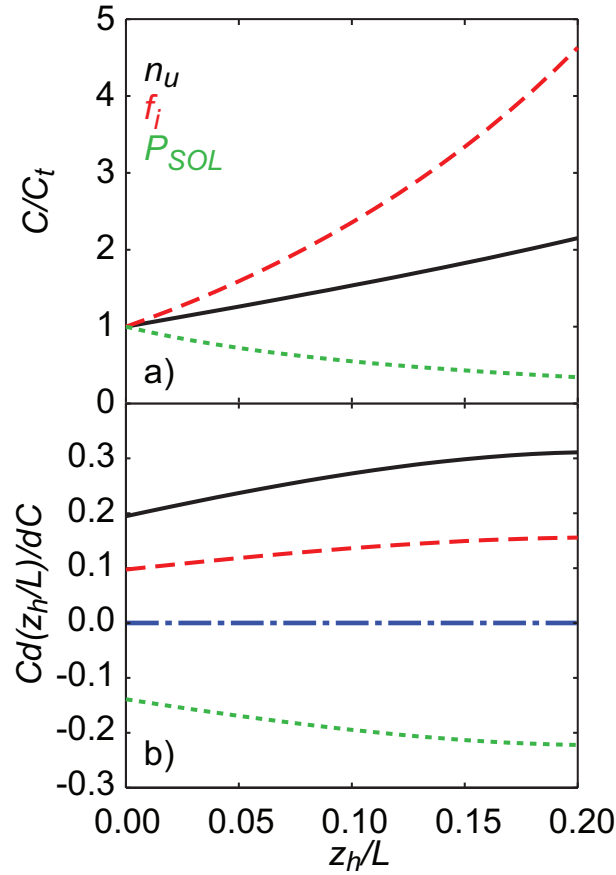
Figure 6. Sensitivity of the detachment front location, z_h/L, to different control variables for the case of $B_\times/B_t = 2$, $z_\times/L = 0.2$: a) The variation in $C/C_t = n_u/n_{ut}$, f_I/f_{It} and $P_{\mathrm{SOL}}/P_{\mathrm{SOL},t}$; b) $C\partial(z_h/L)/\partial C$ as a function of z_h/L.

where in the divertor control is most difficult as well as development of detachment control algorithms.

Recognizing from equation (19) that

$$\frac{dB_h}{dz_h} = \frac{B_\times}{z_\times}\left(1 - \frac{B_t}{B_\times}\right), \tag{32}$$

we can differentiate equation (30) to deduce the general sensitivity of z_h to control parameter $C = [n_u, f_I, P_{\mathrm{SOL}}(\text{or } S_0)]$ (recall $\beta = [1, 2, -7/5]$ respectively) after some algebra

$$\frac{C}{L}\frac{\partial z_h}{\partial C} = \frac{1}{\beta}\Bigg\{\left(1 - \frac{B_t}{B_\times}\right)\frac{B_\times}{B_h}\frac{L}{z_\times}$$

$$+ \frac{2}{7}\left[\frac{z_\times - z_h}{3L}\left(1 + \left|\frac{B_h}{B_\times}\right| + \left|\frac{B_h}{B_\times}\right|^2\right) + \frac{L - z_\times}{2L}\right]^{-1}\left|\frac{B_h}{B_\times}\right|^2\Bigg\}^{-1}. \tag{33}$$

Again, the first term inside the square brackets can be neglected with respect to $(L - z_\times)/2$ when both $B_t^2/B_\times^2$ and $z_\times/L$ are small.

The variation, as a function of z_h, of C/C_t is shown in figure 6a, and its inverse logarithmic derivative in figure 6b. As before, C_t is the value of C when the front is at the target. The parameters used are $B_\times/B_t = 2$ and $z_\times/L = 0.2$. The front moves

furthest (in z_h) for a relative variation in the control parameter C when $|C\partial(z_h/L)/\partial C|$ is the largest. As expected, the sensitivity of the detachment front location to f_I is weaker than for n_u. For P_{SOL} the derivative is negative. The front is most sensitive to relative variations of n_u, particularly for z_h near $z_\times$. This makes it a powerful control for adjusting z_h, but equally it means that one will not be able to allow large relative changes in n_u without exceeding the detachment window.

The detailed shape of the curves in figure 6 depends on the details of the spatial variation of B between x-point and target, which we chose to model here as linear. Other choices will produce different sensitivities as a function of z_h but little change in the detachment window.

6. Discussion

6.1. Relation to the Two-Point model

The "two-point model"[47, 48, 49, 50], which uses one-dimensional parallel heat conduction and pressure balance to relate the upstream and target temperatures and densities, is often used as a robust guide to divertor physics. Since the present treatment uses the same two assumptions, it is closely related. While the two-point model assumes a fixed level of radiated power, our model self-consistently includes radiative loss controlled by temperature, and, in effect, allows the lower-temperature control point (detachment front) to move self-consistently.

Nevertheless, using the two-point model at fixed low target temperature (corresponding to the onset of detachment) one can deduce the upstream density threshold for detachment to start at the target as $n_{ut} \propto P_{\mathrm{SOL}}^{5/7}/L^{2/7}$, which is the same dependence as equation (27). Following the analysis of the effect of changing B on the super-x divertor[55], the classic two-point model has recently been extended[56, 57] to include B magnitude variation (expressed as major radius variation), which introduces an additional factor so that $n_{ut} \propto B_t P_{\mathrm{SOL}}^{5/7}/L^{2/7}$. The B factor is also present in (27), evaluated at $z_h = 0$, $B = B_t$, and for the same reasons: total flux expansion increases the flux-tube area and reduces the flux density $q_\parallel$ for given power flow. Of course, what the two-point model cannot do is calculate the detachment front location as a function of control parameters, nor when the detachment front reaches the x-point. Those are the achievements of the present work, and paper [1].

The concept of a 'virtual target' has been discussed by several authors [31, 58, 59]. Modelling has shown that at the interface between ionization and recombination regions [31] leads to Mach numbers approaching one and a large fraction of ions are 'recycled' as neutrals in the recombination region. The implication is that the temperature at the virtual target is always low and the pressure is constant from virtual target to upstream thus allowing the 2-point model to be used to relate the upstream and target conditions in the usual way [59]. The above characteristics of the virtual target are consistent with our model because T_c is low and essentially fixed as the front moves. In addition we explicitly specify that pressure is constant from z_c to L. Furthermore, the virtual target does not affect stability because we assume the convective energy flux to be small. In

terms of the 2-point model, we are assuming that the radiated fraction $f_{\rm rad}$ is very close to unity.

6.2. Intuitive considerations of the thermal front extent, volume and magnitude of radiation

Implicit to our analysis is the supposition that the front extent, meaning the distance between the T_h and T_c positions, $\Delta z_f = z_h - z_c$, is small compared with L and $z_\times$. Therefore the value and scaling of the front extent is important. That extent can be obtained using equation (8) for the heat flux $q = -\kappa(dT/dz)$ inside the front to write

$$\frac{dz}{dT} = -\frac{\kappa}{q} \simeq \kappa \left[2f_I p^2 \int_{T_c}^{T} \kappa(T') \frac{Q(T')}{T'^2} dT' \right]^{-1/2}, \tag{34}$$

where we have neglected $q_c \ll q$. Integrating equation (34) from T_c to T_h, we obtain

$$\Delta z_f = z_h - z_c = -\int_{T_c}^{T_h} \frac{\kappa(T')}{q(T')} dT'$$

$$\simeq \int_{T_c}^{T_h} \left[2f_I p^2 \int_{T_c}^{T'} \kappa(T'') \frac{Q(T'')}{T''^2} dT'' \right]^{-1/2} \kappa(T') dT'. \tag{35}$$

The exact value of Δz_f depends upon the shape of the radiation coefficient $Q(T)$ as well as other parameters. In order of magnitude, $\Delta z_f \approx \kappa_h T_h/|q| \approx \kappa_1 T_h^{7/2}/|q|$. Assuming T_h of 65 eV, consistent with our Figure 1, with nitrogen as the impurity, and $|q| = 500$ MW/m², Δz_f is of order 9 meters; that overestimates, by a factor of, 3 the exact calculation given by equation (35) and its prediction shown in our Fig. 1. This Δz_f estimate depends sensitively on the value adopted for T_h, which should be taken to be at least 30 eV for Carbon and Nitrogen impurity radiation. We do not consider higher Z impurities because a) they radiate in the SOL more towards the midplane (e.g. Ne) and b) inside the separatrix (e.g. Ne and Ar), thus violating our assumption that the thermal front width be small compared to z_x or L. The effect of b) can be included implicitly in our model through lower $P_{\rm SOL}$.

We can make a more accurate estimation of the dependence of Δz_f on heat flux and position. Using $\kappa = \kappa_1 T^{5/2}(B_\times/B)^2$, equation (35) gives $\Delta z_f \propto p^{-1} f_I^{-1/2}(B_\times/B(z_h))$. According to equation (14), $|q_i| = |q_f| \propto p f_I^{1/2}(B_\times/B(z_h))$, leading to

$$\Delta z_f \propto \frac{B_\times^2}{B^2(z_h)|q_i|} = \frac{B_\times}{B(z_h)|q_\||}. \tag{36}$$

Recall that z is proportional to the volume of the flux tube, and for this reason, $\Delta z_f = z_h - z_c$ *is proportional to the volume of the thermal front (radiating volume).* We can also calculate the parallel and poloidal length of the front using the definition of z in equation (4). Assuming that the poloidal and total magnetic field do not change appreciably across the front, equation (4) gives $\Delta z_f = (B_\times/B(z_h))\Delta l_f = (B_\times/B_p(z_h))\Delta l_{pf}$, where $\Delta l_f = l_h - l_c$ and $\Delta l_{pf} = l_{ph} - l_{pc}$ are the parallel and poloidal length of the front, respectively. Using these results and equation (36), we obtain

$$\Delta l_f \propto \frac{B_\times}{B(z_h)|q_i|} = \frac{1}{|q_\||}, \quad \Delta l_{pf} = \frac{B_p(z_h)}{B(z_h)} \Delta l_f. \tag{37}$$

We expect Δl_{pf} to be ≈ 10 times smaller than Δz_f for typical values of B_p/B.

Equation (36) gives the dependence of the radiating volume on heat flux (and hence P_{SOL}) and magnetic field magnitude $B(z_h)$. Note that it depends on n_u, f_I, or P_{SOL} only indirectly, through $|q_i|$ and z_h: it depends on P_{SOL} through $|q_i|$ and z_h, and on n_u and f_i only through z_h (recall that the position of the front z_h is determined by equation (27)). The inverse dependence on $|q_i|$ is at first sight counter-intuitive. It says that higher parallel heat flux (density) leads to smaller front volume, whereas one might have supposed that higher flux would require a larger front to dissipate it. The explanation is that (for constant field-line geometry and $B_\times/B_t$) if S_0 and hence P_{SOL} is increased, increasing the upstream power flux $|q_i|$, then it is necessary that either n_u or f_I increase to keep the thermal front at a particular position (balancing $q_f = q_i$). Consequently the radiative power *density* in the front increases; and it increases *faster* than the upstream heat flux, hence shortening the volume required to radiate $|q_i|$ away. It is also possible to explain the decrease in front width with increasing heat flux by considering the physics inside the front. As the parallel heat flux is increased, $|dT/dz|$ must increase as well, but the total temperature jump in the front is fixed to be $\Delta T = T_h - T_c$. Thus, the only way for the gradient to increase is to decrease the front width Δz_f.

Our model does show that longer field lines detach more easily; but the reason is not simply an increase in radiating volume. It is a more subtle effect of the overall heat conduction solution. In the present analysis it is represented by the large square bracket factor $[...]^{-2/7}$ in equation (27), which says that the upstream density required for detachment decreases with an increase in L because the upstream temperature in equation (23), whose product with n_u gives pressure, increases with $L^{2/7}$ (recall that in equation (27), for constant P_{SOL}, $S_0(L - z_\times) = P_{\text{SOL}}/(2\pi R \lambda_q (B_p/B_\times))$ is independent of L). That is an effect of conduction changing upstream pressure, not of radiating volume increase.

Total flux expansion ($B_\times/B_t > 1$), by contrast, *does* increase the radiating volume $\Delta z_f \propto 1/B^2$, given that both the cross-sectional area and the radiating parallel distance ($\Delta l_f \propto 1/B$) increase as $1/B$. Given that the total radiation increases as $q_f \propto 1/B$, the emissivity within the thermal front drops $\propto B$. The increase in radiating volume gives an intuitive explanation of the stabilizing effect of decrease in B along the field line. If pressure remains constant, a front that moves toward lower B radiates more power because of an increase of the radiating volume. If the motion towards lower B is also in the direction of decreasing temperature (i.e. $dB/dz > 0$ in our convention) the dissipation power increase *resists* the motion because increases of dissipation tend to make the front move towards higher temperature. If $dB/dz < 0$, as for the typical inner divertor leg, the front would be destabilized. The stability criterion $dB/dz > 0$ is consistent with the general stability condition (13) in our case because $dq_i/dz = 0$ and $|q_f| \propto 1/B$.

The ratio of front extent to field line length is inversely proportional to $|q_i|L$. Therefore this fractional front extent becomes small at high $q_\parallel$ and large L. Future high-performance experiments will therefore have increasingly localized thermal fronts. Although present high-$q_\parallel$ tokamaks can experience localized fronts, linear "divertor simulators" are very unlikely to reach the values of $q_\parallel L$ needed to localize the front.

6.3. Emission localization, neutrals and multidimensional effects

The one-dimensional conduction approximation used here offers a valuable way to understand the nonlinear dynamics of detachment fronts. Its capability to predict both the relative effectiveness of different detachment control variables, and the effect of divertor configuration, is built on a number of simplifications that we review here for clarity. Our treatment includes only energy transport and that strictly through parallel conduction, ignoring convection. Only energy sources due to cross-field transport depend explicitly on position, while energy sinks due to impurities and neutrals are dependent on position only through the temperature variation; in reality, both sinks and sources can be locally enhanced e.g at surfaces where recycling and impurity sources are localized. The lack of direct inclusion of neutrals also means that our model does not describe the effect of detachment front location on divertor neutrals which several authors have pointed out as important for the divertor solution [24, 33, 36].

Electron heat conduction is not always a complete description of parallel heat flow. There is evidence in prior and existing experiments that sometimes substantial heat flux passes through into the cold side of the radiation front [60, 31, 34, 36]. Because electron thermal conduction is small at low temperature, convective heat transport by net particle flow along the field is suggested as the reason for the measured heat fluxes [60]. The effect of this convective transport is to extend the region of radiative losses more than is permitted by pure conduction, enhancing the effective front dissipation, perhaps by a very substantial factor, by maintaining the temperature (and hence radiative loss) higher over a larger volume extending towards the target. We feel that such an enhancement of losses as well as their localization may quantitatively change the model scalings but not the qualitative results (e.g. effect of magnetic field variation) and relative effectiveness of the various control variables. Even though the above shortcomings could be addressed as ad hoc modifications to our model, it is probably more appropriate to pursue them with 2D simulations that include more detailed physics.

Figure 2 implies that once the detachment front reaches the region of decreasing $|q_i|$ above the x-point there is no stable solution and poloidal detachment [61] would ensue. A possible explanation of why this does not often happen in experiments is given in the discussion of MARFEs in reference [1]; conservation of particles in the flux surface was invoked to argue that a cold detached region in a closed field line would deplete the hot region of particles, decreasing the overall pressure and hence the radiation.

Since the equilibrium radiation function Q, without neutral enhancement, is known for specific atomic species [40], a number of authors [42, 44, 43, 41] have made quantitative estimates of the maximum parallel heat flux that can be dissipated in the front. For example [1], $|q_f| \simeq 0.6$ GW/m^2 for Carbon in coronal equilibrium, $n_u = 10^{20}$ m^{-3}, $T_u = 100$ eV and $f_I = 0.04$. This value is less than the SOL power density currently predicted for ITER, motivating investigations of whether additional atomic physics or variations in divertor geometry could further enhance the level of parallel heat flux that can be detached. That is why 2D effects due to cross-field transport [38, 39, 36, 13], which are likely significant, as well as the role of configuration, would need to be included in models to determine whether detachment was possible for a specific case.

6.4. Applications of our model

The results from this study have implications in several areas. One near-term application of the model is for detachment feedback control, which is important for studying the role of detachment location on the tradeoff between maximizing core confinement and minimizing the divertor heat loads and erosion. Early feedback algorithms for impurity seeding control of detachment were fairly simple – e.g. stopping the seed gas injection when the radiation increases at some location[7], or limiting the overall radiated power fraction and/or the neutral flux density in the divertor[6]. Kallenbach has more recently developed a more sophisticated feedback algorithm[25, 26, 4] based on radiation in the core and divertor regions as well as thermoelectric currents at the outer divertor. The more variables (P_{SOL}, impurity seeding and fueling) that are included in the control model of the front location the more easily variations in the core plasma conditions can be handled. Finally, improvements in the characterization of $\partial z_h / \partial C$, e.g. through using 2D codes to include additional sources and sinks, or comparing experimental-derived $\partial z_h / \partial C$ to our model, will improve the fidelity of detachment front location control. Of course improved models are most helpful if we also have better real-time measurements of the detachment front location than currently available.

Beyond enhancements in detachment front control, the enlargement of the detachment window leads to the capability of the divertor plasma to absorb variations in upstream conditions (e.g. transients such as H-L transitions) without either loss of detachment or the detachment front reaching the x-point. Said another way, the divertor plasma can temporarily absorb transients until the feedback system has time to respond. This 'shock absorber' or 'springiness' of the divertor plasma, which is enhanced by increasing $B_\times / B_t$ (and to a lesser extent, $z_\times / L$) is very attractive for a reactor.

A longer-term application of the ideas in the model is to DEMO, and future tokamak design. Enhancing $B_\times / B_t$ as much as possible, consistent with engineering contraints should be pursued for both control and added radiation. If it becomes clear through experiments that λ_q in a reactor will really be of order a mm and/or enhanced control is required, then the benefits brought by maximizing $B_\times / B_t$ may be required, as opposed to a choice. We also note that our model indicates that typical inner divertor configurations lead to poorer, or lack of control of detachment there and little radiating volume. Such effects could be counteracted by bringing the inner divertor leg to lower field regions (e.g. 'double-decker' [62]) and should be explored in code and experiment given the potential to improve detachment control and radiation.

Nothing about our analysis presupposes axisymmetry. It therefore applies equally well to non-axisymmetric magnetic configurations like stellarators, which face many challenges similar to tokamaks in power outflow management. If stellarators can be designed in which the total magnetic field decreases following a field-line away from the confined region into a non-axisymmetric divertor, then they will receive the same benefits of stabilization and control of any detachment region extent that we have shown exist for tokamaks.

Our model may also have applications beyond fusion. The fundamental physics of how plasma temperature and density gradients can be supported along B (thermal

fronts) has much in common with astrophysical and solar plasmas where the high density regions, corresponding to the tokamak divertor plasma, are known as 'condensations'[63]. Direct connections have been made between the condensations in solar prominences[64] and tokamak plasmas, specifically MARFEs (see [45] and references in [46]), which have much in common with divertor detachment. More recent studies of solar prominences[65, 66, 67], as well as coronal rain [68], provide evidence of density and temperature gradients along coronal loops with the highest densities and lowest temperatures farthest from the source of heat/energy (tokamak core plasma or chromosphere). Those same studies show movement of condensed (high-density, low-temperature) regions from the top of the coronal loop to the chromosphere. Our model of the detachment front location should be applicable to such situations which also have B varying along the flux tube.

7. Summary

In this study we use an analytic 1D model to establish the range of different control variables over which a detachment front remains in the divertor between target and x-point: the 'detachment window'. We find that amongst the control variables studied, the impurity fraction f_I possesses a larger normalized detachment window than the upstream density n_u and the scrape-off-layer power P_{SOL}. Thus, the position of the detachment thermal front is most sensitive to changes in n_u, with decreasing sensitivity to P_{SOL} and then f_I. We also find that the detachment window for all control variables is increased (equivalent to making the front location less sensitive to control variables) as the ratio of the total magnetic field at the x-point to that at the target, $B_\times/B_t$, (total flux expansion) is increased. Increasing flux tube length in the divertor, typically through poloidal flux expansion, also increases the detachment window of operation, but significantly less than for increases in $B_\times/B_t$. Characterizing the sensitivity of the detachment front location z_h to a control variable C, we find that $\partial z_h/\partial C$ has substantial variation as a function of position of the detachment front. The model also leads to the conclusion that the size of the radiating volume is not dependent on flux tube length (through poloidal flux expansion or extending the divertor length). However, both the size of the radiation region, as well as the total radiation in it, are increased by total flux expansion as included in the model through $B_\times/B_t > 1$. The simple physics-based model presented here may be useful as a basis for developing better detachment control utilizing multiple control variables, and organizing experiments to study detachment physics. We also feel that it can be applicable to the divertor region of Stellarator fusion devices as well as solar prominences and coronal rain.

8. Acknowledgements

References

[1] I. H. Hutchinson. Thermal front analysis of detached divertors and MARFEs. *Nuclear Fusion*, 34(10):1337–48, 1994.

[2] B. Lipschultz, B. LaBombard, J.L. Terry, C. Boswell, and I.H. Hutchinson. Divertor physics research on Alcator C-Mod. *Fusion Science & Technology*, 51:369–389, 2007.

[3] J Neuhauser, M Alexander, G Becker, H S Bosch, K Buchl, D Coster, R Dux, A Field, S Fiedler, Ch Fuchs, O Gehre, O Gruber, G Haas, A Herrmann, S Hirsch, A Kallenbach, M Kaufmann, K Lackner, G Lieder, K F Mast, V Mertens, H Murmann, B Napiontek, R Neu, F Ryter, H Salzmann, R Schneider, J Schweinzer, M Sokoll, K H Steuer, J Stober, W Suttrop, M Weinlich, U Wenzel, H P Zehrfeld, H Zohm, M Albrecht, K Asmussen, K Behler, K Behringer, M Bessenrodt-Weberpals, M Brambilla, A Carlson, R Chodura, L Cupido, H J DeBlank, S De Pena Hempel, S Deschka, C Dorn, R Drube, W Engelhardt, H U Fahrbach, H U Feist, G Fieg, G Fussmann, C Garcia-Rosales, J Gernhardt, W Herrmann, P Ignacz, B Juttner, W Junker, T Kass, W Koppendorfer, H Kollotzek, K Krieger, B Kurzan, P Lang, R Lang, M Laux, M E Manso, M Maraschek, P McCarthy, D Meisel, R Merkel, D Naujoks, G Neu, M Niethammer, J M Noterdaeme, G Pautasso, C S Pitcher, W Poschenrieder, G Raupp, H Rohr, J Roth, W Sandmann, H B Schilling, M Schittenhelm, H Schneider, W Schneider, K Schonmann, G Schramm, U Seidel, F Serra, A Silva, E Speth, A Stabler, B Streibl, W Treutterer, M Troppmann, M Ulrich, et al. The compatibility of high confinement times and complete divertor detachment in ASDEX-Upgrade. *Plasma Physics and Controlled Fusion*, 37(11A):A37, 1995.

[4] A. Kallenbach, M. Bernert, M. Beurskens, L. Casali, M. Dunne, T. Eich, L. Giannone, A. Herrmann, M. Maraschek, S. Potzel, F. Reimold, V. Rohde, J. Schweinzer, E. Viezzer, M. Wischmeier, and the ASDEX Upgrade Team. Partial detachment of high power discharges in ASDEX upgrade. *Nuclear Fusion*, 55(5):053026, 2015.

[5] The JET Team. Highly radiating and detached plasmas on carbon and beryllium targets. *Plasma Physics and Controlled Fusion*, 37(11A):A227, 1995.

[6] A. Kallenbach, R. Dux, V. Mertens, O. Gruber, G. Haas, M. Kaufmann, W. Poschenrieder, F. Ryter, H. Zohm, M. Alexander, K.H. Behringer, M. Bessenrodt-Weberpals, H.-S. Bosch, K. Buchl, A.R. Field, J.C. Fuchs, O. Gehre, A. Herrmann, S. Hirsch, W. Koppendorfer, K. Lackner, K.F. Mast, G. Neu, J. Neuhauser, S. De Pena Hempel, G. Raupp, K. Schonmann, A. Stabler, K.-H. Steuer, O. Vollmer, M. Weinlich, W.P. West, and T. Zehetbauer. H mode discharges with feedback controlled radiative boundary in the ASDEX Upgrade tokamak. *Nuclear Fusion*, 35(10):1231, 1995.

[7] J. A. Goetz, B. LaBombard, B. Lipschultz, C. S. Pitcher, J. L. Terry, C. Boswell, S. Gangadhara, D. Pappas, J. Weaver, B. Welch, R. L. Boivin, P. Bonoli, C. Fiore, R. Granetz, M. Greenwald, A. Hubbard, I. Hutchinson, J. Irby, E. Marmar, D. Mossessian, M. Porkolab, J. Rice, W. L. Rowan, G. Schilling, J. Snipes, Y. Takase, S. Wolfe, and S. Wukitch. High confinement dissipative divertor operation on Alcator C-Mod. *AIP. Physics of Plasmas*, 6(5):1899–906, 1999.

[8] N. Asakura, N. Hosogane, K. Itami, A. Sakasai, S. Sakurai, K. Shimizu, M. Shimada, H. Kubo, S. Higashijima, H. Takenaga, H. Tamai, S. Konoshima, T. Sugie, K. Masaki, Y. Koide, O. Naito, H. Shirai, T. Takizuka, T. Ishijima, S. Suzuki, and A. Kumagai. Role of divertor geometry on detachment and core plasma performance in JT60U. *Journal of Nuclear Materials*, 266(269):182–8, 1999.

[9] A. Loarte. Effects of divertor geometry on tokamak plasmas. *Plasma Physics & Controlled Fusion*, 43(6), 2001.

[10] J. Rapp, P. Monier-Garbet, G.F. Matthews, R. Sartori, P. Andrew, P. Dumortier, T. Eich, W. Fundamenski, M. von Hellermann, J. Hogan, L.C. Ingesson, S. Jachmich, H.R. Koslowski, A. Loarte, G. Maddison, D.C. McDonald, A. Messiaen, J. Ongena, V. Parail, V. Philipps,

G. Saibene, B. Unterberg, and JET EFDA Contributors. Reduction of divertor heat load in JET ELMy H-modes using impurity seeding techniques. *Nuclear Fusion*, 44(2):312, 2004.

[11] G.P. Maddison, C. Giroud, G.K. McCormick, J.A. Alonso, B. Alper, G. Arnoux, P.C. da Silva Aresta Belo, M.N.A. Beurskens, A. Boboc, S. Brezinsek, I. Coffey, S. Devaux, T. Eich, W. Fundamenski, D. Harting, A. Huber, S. Jachmich, I. Jenkins, E. Joffrin, M.A.H. Kempenaars, M. Lehnen, T. Loarer, P.J. Lomas, A.G. Meigs, P.D. Morgan, V. Riccardo, F.G. Rimini, M.F. Stamp, G. Telesca, H. Thomsen, and JET EFDA contributors. Moderation of divertor heat loads by fuelling and impurity seeding in well-confined ELMy H-mode plasmas on JET. *Nuclear Fusion*, 51(4):042001, 2011.

[12] C. Giroud, G. Maddison, K. McCormick, M.N.A. Beurskens, S. Brezinsek, S. Devaux, T. Eich, L. Frassinetti, W. Fundamenski, M. Groth, A. Huber, S. Jachmich, A. Järvinen, A. Kallenbach, K. Krieger, D. Moulton, S. Saarelma, H. Thomsen, S. Wiesen, A. Alonso, B. Alper, G. Arnoux, P. Belo, A. Boboc, A. Brett, M. Brix, I. Coffey, E. de la Luna, D. Dodt, P. De Vries, R. Felton, E. Giovanozzi, J. Harling, D. Harting, N. Hawkes, J. Hobirk, I. Jenkins, E. Joffrin, M. Kempenaars, M. Lehnen, T. Loarer, P. Lomas, J. Mailloux, D. McDonald, A. Meigs, P. Morgan, I. Nunes, C. Perez van Thun, V. Riccardo, F. Rimini, A. Sirinnelli, M. Stamp, I. Voitsekhovitch, and JET EFDA Contributors. Integration of a radiative divertor for heat load control into JET high triangularity ELMy H-mode plasmas. *Nuclear Fusion*, 52(6):063022, 2012.

[13] F. Reimold, M. Wischmeier, M. Bernert, S. Potzel, A. Kallenbach, H.W. Müller, B. Sieglin, U. Stroth, and the ASDEX Upgrade Team. Divertor studies in nitrogen induced completely detached H-modes in full tungsten ASDEX Upgrade. *Nuclear Fusion*, 55(3):033004, 2015.

[14] B. Lipschultz, J. Goetz, B. LaBombard, G. McCracken, J. Terry, D. Jablonski, C. Kurz, A. Niemzcewski, and J. Snipes. Plasma-surface interactions in the Alcator C-Mod tokamak. *Journal of Nuclear Materials*, 220(222):967–70, 1995.

[15] G. M. McCracken, B. Lipschultz, B. Labombard, J. A. Goetz, R. S. Granetz, D. Jablonski, S. Lisgo, H. Ohkawa, P. C. Stangeby, and J. L. Terry. Impurity screening in Ohmic and high confinement (H-mode) plasmas in the Alcator C-Mod tokamak. *Physics of Plasmas*, 4(5):1681–9, 1997.

[16] A. Niemczewski, I. H. Hutchinson, B. LaBombard, B. Lipschultz, and G. M. McCracken. Neutral particle dynamics in the Alcator C-Mod tokamak. *Nuclear Fusion*, 37(2):151–63, 1997.

[17] F. Reimold, M. Wischmeier, M. Bernert, S. Potzel, D. Coster, X. Bonnin, D. Reiter, G. Meisl, A. Kallenbach, L. Aho-Mantila, and U. Stroth. Experimental studies and modeling of complete H-mode divertor detachment in ASDEX Upgrade. *Journal of Nuclear Materials*, 463(0):128–134, 2015.

[18] N. Richard, B. Terreault, E. Haddad, J. Gunn, G. Abel, S. Chiu, J. L. Gauvreau, H. H. Mai, and W. W. Zuzak. Retention of Ne and N2 in the closed and pumped TdeV divertor with attached and detached plasmas. *Journal of Nuclear Materials*, 241–243(0):760–764, 1997.

[19] J. A. Goetz, B. Lipschultz, C. S. Pitcher, J. L. Terry, P. T. Bonoli, J. E. Rice, and S. J. Wukitch. Impurity compression and enrichment studies on Alcator C-Mod. *Journal of Nuclear Materials*, 266(269):354–9, 1999.

[20] A. Sakasai, H. Takenaga, N. Hosogane, S. Sakurai, N. Akino, H. Kubo, S. Higashijima, H. Tamai, N. Asakura, K. Itami, and K. Shimizu. Helium exhaust in ELMy H-mode plasmas with W-shaped pumped divertor of JT-60U. *Journal of Nuclear Materials*, 266–269(0):312–317, 1999.

[21] H. S. Bosch, W. Ullrich, D. Coster, O. Gruber, G. Haas, J. Neuhauser, R. Schneider, and R. Wolf. Helium transport and exhaust with an ITER-like divertor in ASDEX upgrade. *Journal of Nuclear Materials*, 290–293(0):836–839, 2001.

[22] M. Groth, P. Andrew, W. Fundamenski, H. Y. Guo, D. L. Hillis, J. T. Hogan, L. D. Horton, G. F. Matthews, A. G. Meigs, P. M. Morgan, M. F. Stamp, and M. von Hellermann. Noble gas enrichment studies at JET. *Journal of Nuclear Materials*, 290–293(0):867–871, 2001.

[23] E.E. Mukhin, R.A. Pitts, P. Andrew, I.M. Bukreev, P.V. Chernakov, L. Giudicotti, G. Huijsmans, M.M. Kochergin, A.N. Koval, A.S. Kukushkin, G.S. Kurskiev, A.E. Litvinov, S.V. Masyukevich, R. Pasqualotto, A.G. Razdobarin, V.V. Semenov, S.Yu. Tolstyakov, and M.J. Walsh. Physical aspects of divertor Thomson scattering implementation on ITER. *Nuclear Fusion*, 54(4):043007, 2014.

[24] A. S. Kukushkin, H. D. Pacher, G. W. Pacher, V. Kotov, R. A. Pitts, and D. Reiter. Consequences of a reduction of the upstream power SOL width in ITER. *Journal of Nuclear Materials*, 438, Supplement:S203–S207, 2013.

[25] A Kallenbach, R Dux, J C Fuchs, R Fischer, B Geiger, L Giannone, A Herrmann, T Lunt, V Mertens, R McDermott, R Neu, T Pütterich, S Rathgeber, V Rohde, K Schmid, J Schweinzer, W Treutterer, and ASDEX Upgrade Team. Divertor power load feedback with nitrogen seeding in ASDEX upgrade. *Plasma Physics and Controlled Fusion*, 52(5):055002, 2010.

[26] A. Kallenbach, M. Bernert, T. Eich, J.C. Fuchs, L. Giannone, A. Herrmann, J. Schweinzer, W. Treutterer, and the ASDEX Upgrade Team. Optimized tokamak power exhaust with double radiative feedback in ASDEX upgrade. *Nuclear Fusion*, 52(12):122003, 2012.

[27] A. G. McLean, A. W. Leonard, M. A. Makowski, M. Groth, S. L. Allen, J. A. Boedo, B. D. Bray, A. R. Briesemeister, T. N. Carlstrom, D. Eldon, M. E. Fenstermacher, D. N. Hill, C. J. Lasnier, C. Liu, T. H. Osborne, T. W. Petrie, V. A. Soukhanovskii, P. C. Stangeby, C. Tsui, E. A. Unterberg, and J. G. Watkins. Electron pressure balance in the SOL through the transition to detachment. *Journal of Nuclear Materials*, 463:533–536, 2015.

[28] D. D. Ryutov. Geometrical properties of a snowflake divertor. *Physics of Plasmas*, 14(6):064502, 2007.

[29] M. Kotschenreuther, P. M. Valanju, S. M. Mahajan, and J. C. Wiley. On heat loading, novel divertors, and fusion reactors. *Physics of Plasmas*, 14(7):072502, 2007.

[30] P. M. Valanju, M. Kotschenreuther, S. M. Mahajan, and J. Canik. Super-X divertors and high power density fusion devices. *Physics of Plasmas*, 16(5):056110, 2009.

[31] A. Kukushkin, H.D. Pacher, M. Baelmans, D. Coster, G. Janeschitz, D. Reiter, and R. Schneider. 2D modelling of radiating divertor regime for ITER. *Journal of Nuclear Materials*, 241-243:268–272, 1997.

[32] V. Kotov and D. Reiter. Two-point analysis of the numerical modelling of detached divertor plasmas. *Plasma Physics and Controlled Fusion*, 51:115002, 2009.

[33] S.I. Krasheninnikov, M. Rensink, T.D. Rognlien, A.S. Kukushkin, J.A. Goetz, B. LaBombard, B. Lipschultz, J.L. Terry, and M. Umansky. Stability of the detachment front in a tokamak divertor. *Elsevier. Journal of Nuclear Materials*, 266-269:251–257, 1999.

[34] S. Nakazawa, N. Nakajima, M. Okamoto, and N. Ohyabu. One-dimensional simulation on stability of detached plasma in a tokamak divertor. *Plasma Physics and Controlled Fusion*, 42:401–413, 2000.

[35] M. Nakamura, Y. Ogawa, N. Shinji, R. Hiwatari, and K. Okano. "Multi-layer" one-dimensional model for stability analysis on partially detached divertor plasmas. *Elsevier. Journal of Nuclear Materials*, 415:S553–S556, 2011.

[36] S. Togo, M. Nakamura, Y. Ogawa, K. Shimizu, T. Takizuka, and K. Hoshino. Effects of neutral particles on the stability of the detachment fronts in divertor plasmas. *Plasma and Fusion Research*, 8:2403096, 2013.

[37] E. Havlickova, W. Fundamenski, F. Subba, D. Coster, M. Wischmeier, and G. Fishpool. Benchmarking of a 1D scrape-off layer code SOLF1D with SOLPS and its use in modelling long-legged divertors. *Plasma Physics and Controlled Fusion*, 55(6):065004, 2013.

[38] S.I. Krasheninnikov. Two-dimensional effects in plasma radiation fronts and radiation front jumps in tokamak divertor plasmas. *Physics of Plasmas*, 4:3741, 1997.

[39] S.I. Krasheninnikov, A.A. Batishcheva, and A.N. Simakov. Radiation fronts in tokamak divertor plasmas. *Physics of Plasmas*, 5:2297, 1998.

[40] D.E. Post, R.V. Jensen, C.B. Tarter, W.H. Grasberger, and W.A. Lokke. Steady-state radiative cooling rates for low-density, high-temperature plasmas. *Atomic Data and Nuclear Data Tables*, 20(5):397–439, 1977.

[41] A Kallenbach, M Bernert, R Dux, L Casali, T Eich, L Giannone, A Herrmann, R McDermott, A Mlynek, H W Müller, F Reimold, J Schweinzer, M Sertoli, G Tardini, W Treutterer, E Viezzer, R Wenninger, M Wischmeier, and the ASDEX Upgrade Team. Impurity seeding for tokamak power exhaust: from present devices via ITER to DEMO. *Plasma Physics and Controlled Fusion*, 55(12):124041, 2013.

[42] L.L. Lengyel. Analysis of radiating plasma boundary layers. Report, Max Planck Institut fur PlasmaPhysik, Sept. 1981 1981.

[43] K. Lackner and R. Schneider. The role of edge physics and confinement issues in the fusion reactor. *Fusion Engineering and Design*, 22(12):107–116, 1993.

[44] D. Post, J. Abdallah, R. E. H. Clark, and N. Putvinskaya. Calculations of energy losses due to atomic processes in tokamaks with applications to the International Thermonuclear Experimental Reactor divertor. *Physics of Plasmas*, 2(6):2328–2336, 1995.

[45] B. Lipschultz, B. LaBombard, E.S. Marmar, M.M. Pickrell, J.L. Terry, R. Watterson, and S.M. Wolfe. MARFE: an edge plasma phenomenon. *Nuclear Fusion*, 24(8):977–989, 1984.

[46] B. Lipschultz. Review of MARFE phenomena in tokamaks. *Journal of Nuclear Materials*, 145(147):15–25, 1987. Plasma Fusion Center, MIT, Cambridge, MA, USA. Using Smart Source Parsing Feb. pp. Netherlands. Seventh International Conference on Plasma-Surface Interactions in Controlled Fusion Devices. Princeton, NJ, USA. Princeton Univ. USDOE. 5-9 May 1986 English.

[47] P.C. Stangeby. Can detached divertor plasmas be explained as self-sustained gas targets? *Nuclear Fusion*, 33(11):1695–705, 1993. TY - JOUR M1 - Copyright 2005, IEE U1 - 4610929 L2 - http://dx.doi.org/10.1088/0029-5515/33/11/I10 U2 - detached divertor plasmas self-sustained gas targets divertor tokamaks electron temperature recycling neutrals charge exchange collisions plasma outflow rate particle confinement time elastic collisions.

[48] G M McCracken and J M Pedgley. Estimates of the maximum radiate power in a tokamak divertor. *Plasma Physics and Controlled Fusion*, 35(2):253, 1993.

[49] B. LaBombard, D. Jablonski, B. Lipschultz, G. McCracken, and J. Goetz. Scaling of plasma parameters in the SOL and divertor for Alcator C-Mod. *Journal of Nuclear Materials*, 220(222):976–81, 1995.

[50] P.C. Stangeby. *The Plasma Boundary of Magnetic Fusion Devices*. Plasma Physics. Taylor & Francis, New York, 2000.

[51] G. Fishpool, J. Canik, G. Cunningham, J. Harrison, I. Katramados, A. Kirk, M. Kovari, H. Meyer, and R. Scannell. MAST-upgrade divertor facility and assessing performance of long-legged divertors. *Journal of Nuclear Materials*, 438, Supplement(0):S356–S359, 2013.

[52] F Hofmann, J B Lister, W Anton, S Barry, R Behn, S Bernel, G Besson, F Buhlmann, R Chavan, M Corboz, M J Dutch, B P Duval, D Fasel, A Favre, S Franke, A Heym, A Hirt, C Hollenstein, P Isoz, B Joye, X Llobet, J C Magnin, B Marletaz, P Marmillod, Y Martin, J M Mayor, J M Moret, C Nieswand, P J Paris, A Perez, Z A Pietrzyk, R A Pitts, A Pochelon, R Rage, O Sauter, G Tonetti, M Q Tran, F Troyon, D J Ward, and H Weisen. Creation and control of variably shaped plasmas in TCV. *Plasma Physics and Controlled Fusion*, 36(12B):B277, 1994.

[53] B. LaBombard, E. Marmar, J. Irby, J.L. Terry, R. Vieira, G. Wallace, D.G. Whyte, S. Wolfe, S. Wukitch, S. Baek, W. Beck, P. Bonoli, D. Brunner, J. Doody, R. Ellis, D. Ernst, C. Fiore, J.P. Freidberg, T. Golfinopoulos, R. Granetz, M. Greenwald, Z.S. Hartwig, A. Hubbard, J.W. Hughes, I.H. Hutchinson, C. Kessel, M. Kotschenreuther, R. Leccacorvi, Y. Lin, B. Lipschultz, S. Mahajan, J. Minervini, R. Mumgaard, R. Nygren, R. Parker, F. Poli, M. Porkolab, M.L. Reinke, J. Rice, T. Rognlien, W. Rowan, S. Shiraiwa, D. Terry, C. Theiler, P. Titus, M. Umansky, P. Valanju, J. Walk, A. White, J.R. Wilson, G. Wright, and S.J. Zweben. ADX: a high field, high power density, advanced divertor and RF tokamak. *Nuclear Fusion*, 55(5):053020, 2015.

[54] M. Kotschenreuther, P. Valanju, B. Covele, and S. Mahajan. Magnetic geometry and physics of advanced divertors: The X-divertor and the snowflake. *Physics of Plasmas*, 20(10):102507, 2013.

[55] M. Kotschenreuther, P. Valanju, S. Mahajan, L.J. Zheng, L.D. Pearlstein, R.H. Bulmer, J. Canik, and R. Maingi. The super X divertor (SXD) and a compact fusion neutron source (CFNS). *Nuclear Fusion*, 50(3):035003, 2010.

[56] P.C. Stangeby. Modified 2 point model of the SOL to allow for variation in R_{target}. http://starfire.utias.utoronto.ca/divimp/publications/2PM-with-R_t-variation-10Aug11-inc.pdf, 2011.

[57] T. W. Petrie, J. M. Canik, C. J. Lasnier, A. W. Leonard, M. A. Mahdavi, J. G. Watkins, M. E. Fenstermacher, J. R. Ferron, R. J. Groebner, D. N. Hill, A. W. Hyatt, C. T. Holcomb, T. C. Luce, R. A. Moyer, and P. C. Stangeby. Effect of separatrix magnetic geometry on divertor behavior

in DIII-D. *Journal of Nuclear Materials*, 438, Supplement:S166–S169, 2013.

[58] R. Schneider, H. S. Bosch, D. Coster, J. C. Fuchs, J. Gafert, G. Haas, A. Herrmann, M. Kaufmann, A. Kallenbach, J. Neuhauser, J. Schweinzer, U. Wenzel, and Asdex Upgrade Teams. Role of divertor geometry on detachment in ASDEX Upgrade. *Journal of Nuclear Materials*, 266269:175–181, 1999.

[59] P. C. Stangeby and A. W. Leonard. Obtaining reactor-relevant divertor conditions in tokamaks. *Nuclear Fusion*, 51(6):063001, 2011.

[60] A. W. Leonard, G. D. Porter, R. D. Wood, S. L. Allen, J. Boedo, N. H. Brooks, T. E. Evans, M. E. Fenstermacher, D. N. Hill, R. C. Isler, C. J. Lasnier, R. D. Lehmer, M. A. Mahdavi, R. Maingi, R. A. Moyer, T. W. Petrie, M. J. Schaffer, M. R. Wade, J. G. Watkins, W. P. West, and D. G. Whyte. Radiative divertor plasmas with convection in DIII-D. *Physics of Plasmas*, 5(5):1736, 1998.

[61] G. M. McCracken, J. Allen, K. Axon, R. Barnsley, S. J. Fielding, D. H. J. Goodall, N. Hawkes, J. Hugill, P. C. Johnson, G. F. Matthews, and C. S. Pitcher. A study of detached plasmas in the DITE tokamak. *Journal of Nuclear Materials*, 145147:181–185, 1987.

[62] S McIntosh, D. Hancock, D Taylor, W Morris, E Surrey, T Todd, G Cunningham, and G. Fishpool. "Engineering Feasibility of the Double Decker Divertor". [FIP/P8-9], paper presented at 25th IAEA Int. Conf. on Fusion Energy Conference St Petersburg 2014.

[63] G Field. Thermal instability. *Astrophysical Journal*, 142:531–567, 1965.

[64] D. McCarthy and J. F. Drake. Nonlinear behavior of the radiative condensation instability. *Physics of Fluids B*, 3(1):22–25, 1991.

[65] D. A. N. Müller, V. H. Hansteen, and H. Peter. Dynamics of solar coronal loops. *Astronomy and Astrophysics*, 411(3):605–613, 2003.

[66] A. De Groof, C. Bastiaensen, D. A. N. Müller, D. Berghmans, and S. Poedts. Detailed comparison of downflows seen both in EIT 30.4 nm and Big Bear H movies. *Astronomy & Astrophysics*, 319-328:319, 2005.

[67] J. T. Karpen, S. K. Antiochos, and J. A. Klimchuk. The origin of high-speed motions and threads in prominences. *The Astrophysical Journal*, 637(1):531, 2006.

[68] P. Antolin, G. Vissers, and L. Van der Voort. On-disk coronal rain. *Solar Physics*, 280:457, 2012.